

A mixture of hidden Markov models to predict the lymphatic spread in head and neck cancer depending on primary tumor location

Roman Ludwig^{1,2}, Julian Brönnimann^{1,2}, Yoel Pérez Haas^{1,2}, Esmée Lauren Looman^{1,2}, Panagiotis Balcermpas², Sergi Benavente¹¹, Adrian Schubert^{3,4,7}, Dorothea Barbatei⁸, Laurence Bauwens⁸, Jean-Marc Hoffmann², Olgun Elicin³, Matthias Dettmer^{6,10}, Bertrand Pouymayou², Roland Giger^{4,5}, Vincent Grégoire⁸, and Jan Unkelbach^{1,2}

¹Department of Physics, University of Zurich, Zurich, Switzerland

²Department of Radiation Oncology, University Hospital Zurich, Zurich, Switzerland

³Department of Radiation Oncology, Bern University Hospital, Bern, Switzerland

⁴Department of ENT, Head & Neck Surgery, Bern University Hospital, Bern, Switzerland

⁵Head and Neck Anticancer Center, Bern University Hospital, Bern, Switzerland

⁶Institute of Tissue Medicine and Pathology, Bern University Hospital, Bern, Switzerland

⁷Department of ENT, Head & Neck Surgery, Réseau Hospitalier Neuchâtelois, Neuchâtel, Switzerland

⁸Department of Radiation Oncology, Centre Léon Bérard, Lyon, France

⁹Department of Head and Neck Surgery, Centre Léon Bérard, Lyon, France

¹⁰Institute of Pathology, Klinikum Stuttgart, Stuttgart, Germany

¹¹Departement of Radiation Oncology, Hospital Vall d'Hebron, Barcelona, Spain

Abstract We previously developed a mechanistic hidden Markov model (HMM) to predict the lymphatic tumor progression in oropharyngeal squamous cell carcinomas. To extend the model to other tumor subsites in the head and neck defined by ICD-10 codes, we develop a mixture model combining multiple HMMs. The mixture coefficients and the model parameters are learned via an EM-like algorithm from a large multi-centric dataset on lymph node involvement. The methodology is demonstrated for tumors in the oropharynx and oral cavity. The mixture model groups anatomically nearby subsites and yields interpretable mixture coefficients consistent with anatomical location. It allows the prediction of differences in lymph node involvement depending on tumor subsite.

1 Introduction

Head and neck squamous cell carcinomas (HNSCC) frequently spread through the lymphatic system [1, 2]. Current diagnostic imaging modalities are unable to detect microscopic lymph node metastases [3, 4]. To avoid nodal recurrences, large volumes in the neck, which are at risk of harbouring occult disease, are irradiated electively. Guidelines about which lymph node levels (LNLs) to irradiate [5] are currently not based on a patient's individual risk, but on the overall prevalence of nodal disease as reported in the literature [1, 2].

To personalize the prediction of the risk for occult disease, given a patient's individual diagnosis, we published

1. large, multi-centric data that reports per patient which LNLs were clinically/pathologically involved [6, 7].

And, building on this work,

2. an interpretable hidden Markov model (HMM), trained with this data, to predict the risk for occult nodal disease, given an individual patient's diagnosis [8].

Such a personalized risk prediction may allow clinicians to safely reduce the elective clinical target volume (CTV-N) and

thus reduce side-effects that degrade the patient's quality of life without compromising treatment efficacy [9].

Here, we extend the previous work by incorporating the primary tumor location (specified as ICD-10 code) into the model of lymphatic tumor progression, focusing on tumors in the oropharynx and the oral cavity. HNSCC patients with primary tumors at different subsites show different patterns of lymphatic spread [1, 2]. So far, this could be handled by training different models for broader categories of tumor locations, e.g. oropharynx and oral cavity tumors. However, this approach does not describe differences in lymphatic spread between different subsites within the oropharynx and oral cavity. To address this issue, we present an approach using mixtures of HMMs. The intuition is that the lymphatic spread of a tumor that lies anatomically at the boarder of oropharynx and oral cavity (e.g. tumors in the palate) may be described by a mixture of different models. Tumor subsites used in this work are sketched in figure 1.

2 Materials and Methods

Each LNL $v \in \{1, 2, \dots, V\}$ considered in our model is represented by a binary random variable X_v representing the true state of that level (0 for "healthy" and 1 for "involved"). A patient's state of lymph node involvement can be represented in a random vector $\mathbf{X} = (X_1, X_2, \dots, X_V)$. When a patient is diagnosed with HNSCC, we only observe the clinical lymph node involvement based on imaging, which we denote as another binary random variable Y_v . To compute the personalized risk of occult disease \mathbf{X} , given a diagnosis \mathbf{Y} , we apply Bayes' law:

$$P(\mathbf{X} | \mathbf{Y}) = \frac{P(\mathbf{Y} | \mathbf{X}) P(\mathbf{X})}{\sum_{\mathbf{X}^*} P(\mathbf{Y} | \mathbf{X}^*) P(\mathbf{X}^*)} \quad (1)$$

In the above equation, the term $P(\mathbf{Y} | \mathbf{X})$ is given by the sen-

sitivity and specificity of the diagnostic procedure. The term $P(\mathbf{X})$ represents the prior probability of involvement, which depends on the probability of the tumor to spread through the lymphatic system. The main task of the HMM is to model $P(\mathbf{X})$ and the main contribution of this paper is to incorporate the primary tumor subsite into the model of $P(\mathbf{X})$.

2.1 Hidden Markov Model for Lymphatic Progression

A patient's state of lymph node involvement $\mathbf{X}[t]$ evolves over discrete time steps t . Let us enumerate all 2^V possible states, representing all combinations of LNLs. In this paper, we consider ipsilateral LNLs I, II, III and IV, which amounts to 16 possible states. The HMM is specified by a *transition matrix*:

$$\mathbf{A} = (A_{ij}) = P(\mathbf{X}[t+1] = \xi_j \mid \mathbf{X}[t] = \xi_i) \quad (2)$$

whose elements A_{ij} contain the conditional probabilities that a state $\mathbf{X}[t] = \xi_i$ transitions to $\mathbf{X}[t+1] = \xi_j$ over one time step. The transition matrix is specified and parameterised via the graphical model shown in figure 1. The red arcs in the graph of figure 1 (right panel) are associated with the probability that the primary tumor spreads directly to a LNL (parameters b_v). The blue arcs describe the spread from an upstream LNL – given it is already metastatic – to a downstream level (parameters $t_{v \rightarrow v+1}$).

Now, let π be the *starting distribution*

$$\pi = (\pi_i) = P(\mathbf{X}[0] = \xi_i) \quad (3)$$

denoting the probability to start in state ξ_i at time step 0. Assuming that every patient started with all LNLs being healthy, we set π_i to zero for all states except the completely healthy state $\xi = (0, 0, 0, 0)$, which has probability one. Using the quantities introduced so far, the probability $P(\mathbf{X}[t] = \xi_i)$ to be in state θ_i in time step t can now be conveniently expressed as a matrix product:

$$P(\mathbf{X}[t] = \xi_i) = (\pi \cdot \mathbf{A}^t)_i \quad (4)$$

This evolution implicitly marginalizes over all possible paths to arrive at state ξ_i after t time-steps. Additionally, we must marginalize over the unknown time of diagnosis using a time-prior $P_T(t)$. This finally defines the probability distribution over all states of lymph node involvement used in equation 1.

$$P(\mathbf{X} = \xi_i \mid \theta) = \sum_{t=0}^{t_{\max}} P_T(t) (\pi \cdot \mathbf{A}^t)_i \quad (5)$$

where $\theta = \{b_v, t_{v \rightarrow v+1}\}$ denotes the set of all model parameters (7 in our case). Fortunately, the exact length and shape of this distribution has little impact as previously shown [8]. We set $t_{\max} = 10$ and $P_{\text{early}}(t)$ to a binomial distribution with parameter 0.3. Further details on the HMM can be found in Ludwig, Pouymayou, Balernpas, et al. [8] and Ludwig [10].

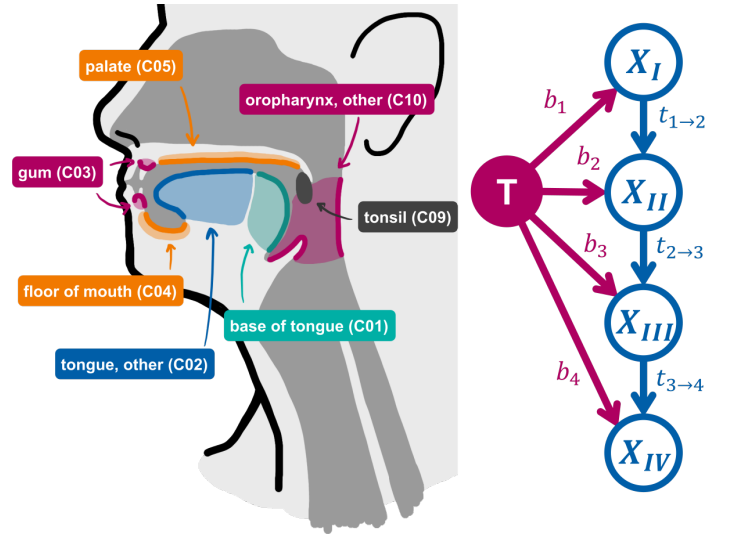


Figure 1: On the left: Anatomical sketch of the tumor subsites and corresponding ICD-10 codes considered in this work. The subsite “other parts of mouth” (C06) was not drawn. On the right: Parametrized graphical model of the lymphatic network considering four LNLs. Blue nodes represent the hidden states of LNLs X_v , while the red one is the tumor. Arcs represent possible routes of metastatic spread, associated with a probability.

2.2 Mixture of HMMs

Let us now assume that primary tumors at different subsites have different patterns of lymphatic spread, corresponding to different model parameters θ . Training a separate model for every possible subsite (ICD-10 code) would require a sufficiently large dataset for every tumor site. However, anatomically nearby locations are expected to show very similar patterns of LNL involvement. Therefore, we consider a mixture model.

Let us assume that we have a dataset \mathbf{D} that is specified via the number of patients N_{is} that were diagnosed in LNL involvement state i and had a primary tumor in subsite s . Let us further assume that we want to describe this dataset using a mixture of M HMMs, each with a different set of model parameters θ_m . As the generative model of the data, we assume that a patient with subsite s is generated with probability π_{sm} from model m . The likelihood of the dataset can then be written as

$$P(\mathbf{D} \mid \theta, \pi) = \prod_s \prod_i \left[\sum_{m=1}^M \pi_{sm} P_m(\mathbf{X} = \xi_i \mid \theta_m) \right]^{N_{is}} \quad (6)$$

We now have two types of parameters, the probabilities of tumor spread for the different models, θ_m , and the mixing coefficients π_{sm} . Assuming a uniform prior in the interval $[0, 1]$ for all parameters, the posterior distribution over the parameters $P(\theta, \pi \mid \mathbf{D})$ is given by the likelihood in equation 6 except for a normalisation constant. In this work, we use Markov chain Monte Carlo sampling (MCMC) via the emcee Python package [11] to sample model parameters

from the posterior distribution. However, $P(\theta, \pi | \mathbf{D})$ itself is a multi-model distribution because one can permute the different models. To address this problem, we revert to an *expectation-maximization (EM)* algorithm where we iterate two steps until convergence of the mixing coefficients. In the E-step, we sample model parameters θ_m using MCMC for given mixing coefficients π_{sm} . In the M-step, we maximize the likelihood with respect to the mixing coefficients for given samples of θ_m .

2.3 Multi-Centric Data

For the analyses in this work, we used five datasets from four different institutions, resulting in 1242 patients in total.

1. 287 oropharyngeal patients from the University of Zurich in Switzerland
2. 263 oropharyngeal patients from the Centre Léon Bérard in France
3. 289 oropharyngeal and oral cavity patients from the Inselspital Bern in Switzerland
4. 239 oropharyngeal and oral cavity patients from the Centre Léon Bérard in France
5. 162 oropharyngeal patients from the Hospital Vall d'Hebron in Spain (not yet public)

The data sets 1-4 are publicly available in the form of CSV tables [7, 12] and may be interactively explored in our **Lymphatic Progression eXplorer** [LyProX](#). For each patient, the primary tumor subsite is reported (among other patient and tumor characteristics) and each individual LNL is reported as metastatic or healthy, according to the available diagnostic modalities (in part pathology after neck dissection, otherwise clinical involvement).

In figure 2, we plot the prevalence of involvement in the four ipsilateral LNLs I, II, III, and IV stratified by the primary tumor's subsite. The figure illustrates the variations in LNL involvement between subsites within the oral cavity and oropharynx categories. The number of patients for each subsite is indicated in figure 3.

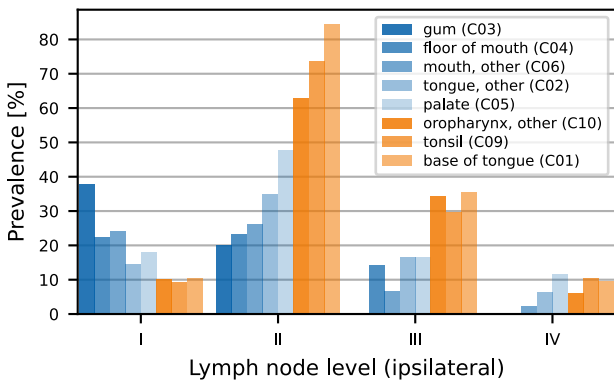


Figure 2: Prevalence of ipsilateral LNL involvement stratified by subsite. The subsites are sorted in ascending order by their prevalence of involvement in LNL II. Oral cavity subsites are plotted in shades of blue, oropharynx subsites in shades of orange.

3 Results

We demonstrate the methodology for a mixture model with $M = 2$ components, considering the ipsilateral involvement of LNLs I, II, III, and IV and the primary tumor subsites shown in figure 2. In figure 3 we show the resulting mixture coefficients π_{sm} . The interpretation of this result is as follows: tumors of the base of tongue (C01) are fully described by component A, and tumors of the gum (C03) are fully described by component B. These two subsites are the most distinct regarding the involvement of LNLs I and II, and the result is thus intuitive. Component A may be interpreted as a model for oropharynx-like tumor spread, and component B as a model for oral cavity-like tumor spread. All other subsites are described as mixtures. tumors in the tonsil (C09) have LNL involvement similar to base of tongue tumors and are mostly assigned to component A. Instead, tumors of the palate (C05) are to similar degree assigned to components A and B, which is consistent with the anatomical location and the observation that the LNL involvement is in between oropharynx and oral cavity-type patterns (figure 2).

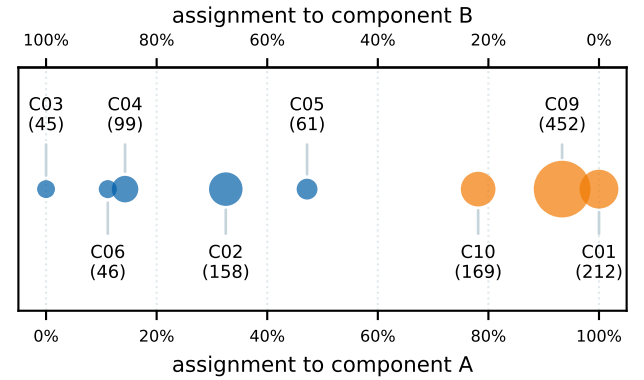


Figure 3: Assignment of each subsite to each of the two components. The further left a subsite, the more it is assigned to component A, the further right, the more to component B. The size of the marker (area) corresponds to the number of patients in the subsite.

The figure 4 illustrates the model's predictions of the overall prevalence of lymph node involvement in LNLs I, II and III (filled histograms) for selected subsites, obtained by summing the probabilities of states where the respective level is involved. The mixture model is compared to two independent HMM models trained for oral cavity and oropharynx (by pooling the respective subsites). The mixture model and the independent oropharynx model perform similarly for tonsil tumors (C09), which is the largest patient group, dominating the independent oropharynx model and the component B in the mixture model. However, the mixture model better predicts the higher prevalence in level II for base of tongue and palate tumors.

4 Discussion

We have previously developed a model of lymphatic progression of HNSCC using HMM, which allows us to estimate

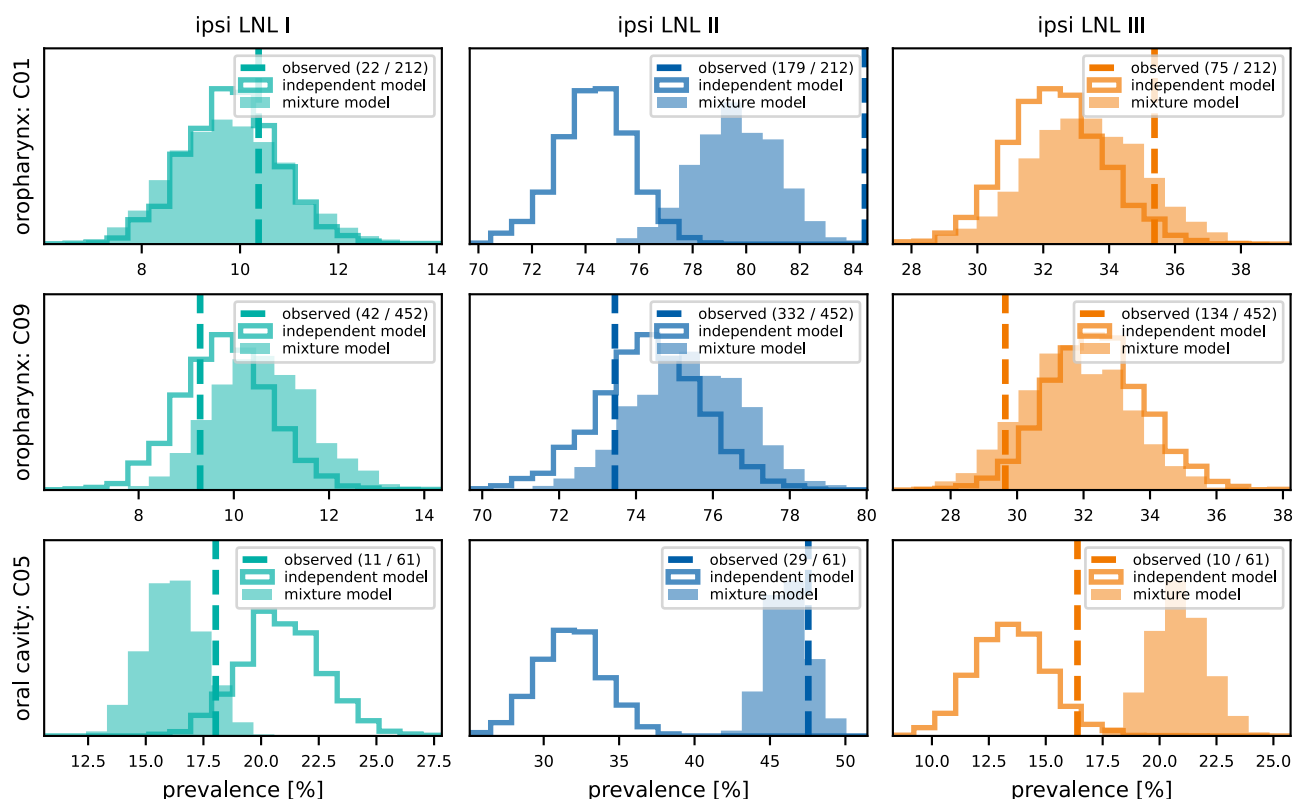


Figure 4: The prevalence of involvement as seen in the data (vertical dashed lines), predicted by an independent model for the oropharyngeal or oral cavity patients (outlined histograms), and predicted by the mixture model (filled histograms). Each row corresponds to one subsite and each column to one LNL.

the probability of occult lymph node metastases in clinically negative LNLs. Mixture models are a suitable method to incorporate the primary tumor location into the model, which allows us to account for differences in lymph node involvement for different subsites. Future work will extend the work to tumors in the hypopharynx and larynx and optimize the number of model components.

Acknowledgements

This work was supported by the clinical research priority program (CRPP) “Artificial intelligence in oncological imaging” of the University of Zurich and by the Swiss cancer research foundation under grant KFS 5645–08–2022.

References

- [1] R. Lindberg. “Distribution of Cervical Lymph Node Metastases from Squamous Cell Carcinoma of the Upper Respiratory and Digestive Tracts”. *Cancer* 29.6 (June 1972), pp. 1446–1449. doi: [10.1002/1097-0142\(197206\)29:6<1446::AID-CNCR2820290604>3.0.CO;2-C](https://doi.org/10.1002/1097-0142(197206)29:6<1446::AID-CNCR2820290604>3.0.CO;2-C).
- [2] J. Woolgar. “Histological Distribution of Cervical Lymph Node Metastases from Intraoral/Oropharyngeal Squamous Cell Carcinomas”. *British Journal of Oral and Maxillofacial Surgery* 37.3 (June 1999), pp. 175–180. doi: [10.1054/bjom.1999.0036](https://doi.org/10.1054/bjom.1999.0036).
- [3] V. Snyder, L. K. Goyal, E. M. R. Bowers, et al. “PET/CT Poorly Predicts AJCC 8th Edition Pathologic Staging in HPV-Related Oropharyngeal Cancer”. *The Laryngoscope* n/a.n/a (Jan. 2021). doi: [10.1002/lary.29366](https://doi.org/10.1002/lary.29366).
- [4] M. P. Strohl, P. K. Ha, R. R. Flavell, et al. “PET/CT in Surgical Planning for Head and Neck Cancer”. *Imaging Options for Head and Neck Cancer* 51.1 (Jan. 2021), pp. 50–58. doi: [10.1053/j.semnuclmed.2020.07.009](https://doi.org/10.1053/j.semnuclmed.2020.07.009).
- [5] J. Biau, M. Lapeyre, I. Troussier, et al. “Selection of Lymph Node Target Volumes for Definitive Head and Neck Radiation Therapy: A 2019 Update”. *Radiotherapy and Oncology* 134 (May 2019), pp. 1–9. doi: [10.1016/j.radonc.2019.01.018](https://doi.org/10.1016/j.radonc.2019.01.018).
- [6] R. Ludwig, J.-M. Hoffmann, B. Pouymayou, et al. “A Dataset on Patient-Individual Lymph Node Involvement in Oropharyngeal Squamous Cell Carcinoma”. *Data in Brief* 43 (Aug. 2022), p. 108345. doi: [10.1016/j.dib.2022.108345](https://doi.org/10.1016/j.dib.2022.108345).
- [7] R. Ludwig, A. Schubert, D. Barbatei, et al. “A Multi-Centric Dataset on Patient-Individual Pathological Lymph Node Involvement in Head and Neck Squamous Cell Carcinoma”. *Data in Brief* (Dec. 2023), p. 110020. doi: [10.1016/j.dib.2023.110020](https://doi.org/10.1016/j.dib.2023.110020).
- [8] R. Ludwig, B. Pouymayou, P. Balermipas, et al. “A Hidden Markov Model for Lymphatic Tumor Progression in the Head and Neck”. *Scientific Reports* 11.1 (Dec. 2021), p. 12261. doi: [10.1038/s41598-021-91544-1](https://doi.org/10.1038/s41598-021-91544-1).
- [9] S. S. Batth, J. J. Caudell, and A. M. Chen. “Practical Considerations in Reducing Swallowing Dysfunction Following Concurrent Chemoradiotherapy with Intensity-Modulated Radiotherapy for Head and Neck Cancer”. *Head Neck* 36 (2014), pp. 291–298. doi: [10.1002/hed.23246](https://doi.org/10.1002/hed.23246).
- [10] R. Ludwig. “Modelling Lymphatic Metastatic Progression in Head and Neck Cancer”. PhD thesis. Zurich: University of Zurich, 2023.
- [11] D. Foreman-Mackey, D. W. Hogg, D. Lang, et al. “Emcee: The MCMC Hammer”. *ψasp* 125.925 (Mar. 2013), p. 306. doi: [10.1086/670067](https://doi.org/10.1086/670067).

- [12] R. Ludwig, J.-M. Hoffmann, B. Pouymayou, et al. “Detailed Patient-Individual Reporting of Lymph Node Involvement in Oropharyngeal Squamous Cell Carcinoma with an Online Interface”. *Radiotherapy and Oncology* 169 (Apr. 2022), pp. 1–7. doi: [10.1016/j.radonc.2022.01.035](https://doi.org/10.1016/j.radonc.2022.01.035).